Polystyrene Chain Geometry Probed by Ion Mobility Mass Spectrometry and Molecular Dynamics Simulations

Sarajit Naskar, Andrea Minoia, Quentin Duez, Aidan Izuagbe, Julien De Winter, Stephen J. Blanksby, Christopher Barner-Kowollik, Jérôme Cornil, and Pascal Gerbaux*

ABSTRACT: Polystyrene (PS) is a thermoplastic polymer commonly used in various applications due to its bulk properties. Designing functional polystyrenes with well-defined structures for targeted applications is of significant interest due to the rigid and apolar nature of the polymer chain. Progress is hindered to date by the limitations of current analytical methods in defining the atomistic-level folding of the polymer chain. The integration of ion mobility spectrometry and molecular dynamics simulations is beneficial in addressing these challenges. However, data on gas-phase polystyrene ions are rarely reported in the literature. We herein investigate the gas phase structure of polystyrene ions with different end groups to establish how the nature and the rigidity of the monomer unit affect the charge stabilization. We find that, in contrast to polar polymers in which the charges are located deep in the ionic globules, the charges in the PS ions are rather located at the periphery of the polymer backbone, leading to singly and doubly charged PS ions adopting dense elliptic-shaped structures. Molecular dynamics (MD) simulations indicate that the folding of the PS rigid chain is controlled by phenyl ring interactions with the charge ultimately remaining excluded from the core of the globular ions, whereas the folding of polyether ions is initiated by the folding of the flexible polyether chain around the sodium ion that remains deeply enclosed in the core of the ions.

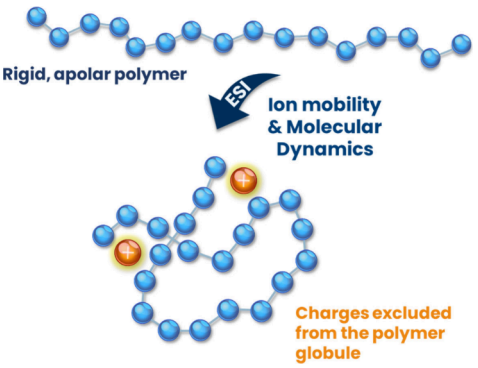

KEYWORDS: *polystyrene, molecular dynamic simulations, ion mobility, density, collisional cross sections, polymer folding*

INTRODUCTION

Mass spectrometry is efficient in deciphering the structural complexity of polymers at the molecular level. The emergence of matrix-assisted laser desorption/ionization (MALDI) and electrospray ionization (ESI) enabled the ionization and transfer of intact compounds to the gas phase[1−4] and allowed for the structural analysis of polymer samples.[5−12] With the use of high-resolution mass spectrometry (HRMS) together with tandem mass spectrometry (MS/MS) experiments, it is possible to identify the nature of the (co)monomer units and end groups, while obtaining information on the arrangement of comonomers within copolymers.[13−16] Ion mobility spectrometry (IMS) coupled to mass spectrometry for polymer characterization is also exploited as an analytical method for the separation of isomeric polymers with different topologies, typically branched or cyclic versus linear polymers,[17−20] complex polymer blends,[21−24] or copolymers.[25−27] IMS experiments entail the introduction of ions in a cell pressurized by a buffer gas (typically He or N_2) under the influence of an electric field. The ions are subsequently separated according to their ion mobility, which correlates with their speed of travel through the cell. The ion mobility directly depends on the charge (z) and the size/shape of the ions (collision cross section, CCS). The CCS itself formally represents a momentum-transfer cross section, which is a temperature-dependent property of the ion-gas system that reflects their interactions.[28−30]

The internal structure of polymer ions cannot be assigned to a single CCS value, and atomistic simulations are mandatory to interpret the gas-phase structure of polymer ions. The comparison between the experimental and theoretical CCS (CCS_{exp} vs CCS_{th}) of MD-simulated structures allows for a selection of candidate ion geometries representing the conformations sampled by IMS-MS. This enables the study of (i) the ion conformations, (ii) the conformational dynamics, and (iii) the nature and strength of the intramolecular interactions.[23,31−37]

Synthetic polymers occupy a unique place in the field of IMS since, due to their intrinsic dispersity, they offer a broad range of homologous ions with different lengths to monitor the size-dependency of the ion CCS.[35,36,38] Most IMS-MS reports

address singly and multiply charged polyethers and polyesters that are readily ionizable by ESI as they form adducts with alkali ions by charge-dipole interactions. The resulting conformations in the gas phase are either globular or "beads-on-a-string" depending on the chain length, charge state, and on the efficiency with which the polymer counterbalances the Coulombic repulsion between charges.[39,40] Even if the ability of the polymer to fold around the metal ion(s) depends on its flexibility, the interaction between the polymer functional groups and the charge(s) always lead to a globular shape for larger chains.[22] Polymers often behave as random coils in solution,[41,42] making the use of IMS irrelevant to study their solution phase structure. On the other hand, peptides in solution for instance can form highly organized structures that are stabilized by strong intramolecular interactions.[43−46] Total or partial retention of solution-phase conformations upon ionization and transfer into the gas phase have been nicely demonstrated for peptides using IMS experiments, unlike floppy polymers.[43,47]

Polystyrene is a thermoplastic polymer commonly used in various applications such as packaging, insulation, medical devices, and electronics, due to its bulk properties such as transparency, low density, rigidity, low thermal conductivity, and low electrical conductivity.[48] Designing functional polystyrenes for targeted applications such as drug encapsulation,[49] cell targeting, and catalysis is of significant interest due to the rigid and apolar nature of the polymer chain.[45] However, progress is hindered by the limitations of current analytical methods in defining the atomistic-level folding and intramolecular cross-linking of the polymer chain. The integration of ion mobility spectrometry (IMS) and molecular dynamics (MD) simulations is highly beneficial for addressing these challenges. However, data on gas-phase polystyrene ions is rarely reported in the literature. While mass spectrometry analyses of polystyrene samples have been conducted, often utilizing Ag^+ to aid cationisation,[50−53] the 3D structure(s) of the resulting ions are far less understood. Bowers and co-workers[54] were one of the few groups to explore the 3D structure of polystyrene ions (with alkali and silver ions) using a combination of IMS-MS and molecular dynamics computations. On the basis of their investigation of oligomers ($DP < 7$) across a range of cationization agents, they proposed a "V" shape for all ion types, including for silver cationized polymers, where the shape is induced by a cationic stacking of styrene moieties.[54]

Herein, as featured in Scheme 1, we critically extend these investigations to much larger polystyrenes and to higher charge states using the unique combination between IMS-MS and MD, with particular emphasis on the impact of the apolar and rigid nature of the polystyrene chain on the charge stabilization in the gas phase of the mass spectrometer.

EXPERIMENTAL SECTION

HPLC grade tetrahydrofuran (>99.8%), acetonitrile (>99.9%), acetone (>99.8%), methanol (>99.8%), toluene (>99.8%), and chloroform (>99.9%) solvents were purchased from Chem-Lab (Zedelgem, Belgium). Silver nitrate (>99%) and sodium iodide were purchased from VWR (Leuven, Belgium) and used without any further purification. Polyethylene glycol was acquired from Sigma-Aldrich and utilized as an IMS-MS calibrant. TEMPO-PS (2,2,6,6-tetramethylpiperidine-*N*-oxyl end group: $Đ = 1.2$ − $M_n = 3400$ g mol^{-1}) was prepared according to literature (see Figure S1 for the ^{1}H NMR spectrum),[55] whereas BU-PS$_{LM}$ and BU-PS$_{HM}$ [sec-butyl end group: $Đ = 1.03$ − $M_n = 3270$ g mol^{-1} (BU-PS$_{HM}$) and $Đ = 1.01$ − $M_n = 580$ g mol^{-1} (BU-PS$_{LM}$)] were purchased from Agilent Technologies (GPC/SEC Calibration Kits). LM and HM in the subscript stand for low mass and high mass, respectively. Agilent BU-PS standards are prepared by living anionic polymerization with a sec-butyl initiating substituent that is attached to the CH_2 group of styrene.[56] The MALDI-ToF analyses of all the polymers are reported in Figures S2−S5 and the mass parameters are gathered in Table S2.

Scheme 1. Folding of Polystyrene (PS) Chains upon Electrospray Ionization: the Primary Objective of This Joint Experimental and Theoretical Investigation Is to Decipher at the Atomistic-Level the Internal Structure of Gaseous PS Ions

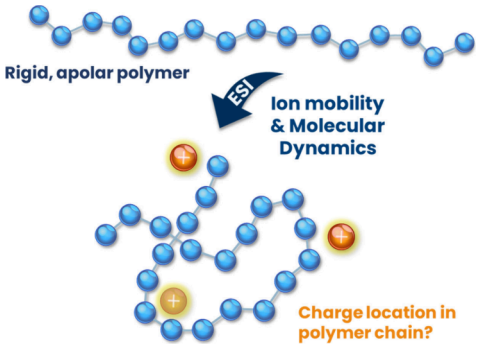

ION MOBILITY EXPERIMENTS

Polystyrene stock solutions of 1.0 mg mL^{-1} were prepared in acetone and acetonitrile (20:80, v/v). TEMPO-PS was analyzed with and without $AgNO_3$ as the cationizing agent. BU-PS$_{LM/HM}$ were only analyzed using $AgNO_3$ as the cationization agent because the lack of the basic functional groups precludes significant protonation under ESI conditions. The $AgNO_3$ solution (10.0 mg mL^{-1}) was prepared in THF and acetonitrile (1:9, v/v), and 2 μL of the cationization agent solution and 1 mL of the polystyrene solution were combined. The PS solutions (with and without $AgNO_3$) were 100 times diluted with acetone and acetonitrile (20:80, v/v) before ESI analysis.

MS spectra and CCS measurements were performed on a Waters Synapt G2-Si mass spectrometer. The solutions were infused at a flow rate of 5 μL min^{-1} with a capillary voltage of 3.1 kV, a source temperature of 100 °C, and a desolvation temperature of 150 °C. The standard IMS-MS parameters were wave height = 40 V, wave velocities = 350 or 600 or 800 m s^{-1}, mass range = m/z 50−4000; N_2 flow rate = 60 mL min^{-1}, He flow rate = 180 mL min^{-1}, and trap bias = 45.0 V. A pre-established calibration procedure[57] was used to convert the experimentally determined arrival time distributions to $^{TW}CCS_{N2\rightarrow He}$,[58] which will be referred to as CCS_{exp}.

MOLECULAR DYNAMICS SIMULATIONS

All calculations were carried out for a run lasting 25 ns with 1 fs time step in the NVT ensemble at 300 K (as temperature does not create much effect due to the high pressure in the IMS chamber) with the Materials Studio software (BIOVIA, San Diego, CA).[59] The PCFF force field was used and validated by the fact that the calculated effective density of TEMPO-PS (0.62−0.66 Da/Å^3) is in good agreement with the

reported density of bulk polystyrene (0.57−0.62 Da/Å^3).[60] At first, a geometrical optimization was performed starting from a linear polymer chain (without charge) using the force field assigned algorithm for charge assignment. The final geometry was further reoptimized after the addition of a charge (H^+ for TEMPO-PS and Ag^+ for BU-PS) to the optimized polymer chain. For the 2+ ions, a second geometry optimization was performed after the addition of the second charge (Ag^+) to the polymer chain. A quenched dynamics was then executed for 20 ns using 1 fs time step and 100 Å van der Waals and electrostatic interaction cutoff at 300 K. A MD run was then performed starting from the most stable structure obtained from the quenched dynamics until the calculated radius of gyration reaches equilibrium. The CCS calculations were carried out by taking average of 400 frames utilizing the trajectory method[61] (TM) model implemented within the Collidoscope software.[62] We also determined the solvent accessible surface area (SASA) and this value against the molecular volume (V_{SASA}) used to estimate the effective density of the PS ions. Note that V_{SASA} was estimated only from the last frame of the dynamics with the Materials Studio 7.0 "Atom Volumes & Surfaces"[59] module using He as the probe. This implies that the SASA value also includes the contribution of the He atom as an additional layer covering the ion surface. The SASA value reflects the rugosity of the surface, except for the small surface irregularities that are too small to be probed by the helium atom. For the investigation of the folding process of PS and PEG ions with DP = 44, we performed a geometry optimization starting from a linear polymer chain (without charge) using the force field assigned charges. After that we performed a second geometry optimization after adding a charge at different positions. Finally, we run a NVT MD simulation for 2 ns at 300 K, using 1 fs time step and 100 Å van der Waals and electrostatic interaction cutoff.

DENSITY FUNCTIONAL THEORY (DFT) CALCULATIONS

Calculations were performed at the density functional theory (DFT) level using a 6-31G** double-ζ basis set and the B3LYP functional, as implemented in the Gaussian 09 (D01 revision) suite, to determine the most favorable protonation center for the TEMPO end group.[63] To describe cation Ag^+-π interactions, the B3LYP functional has been used together with a cc-pVTZ basis set for carbon and hydrogen and a LANL2DZ basis set for silver ion,[64] respectively. To properly describe the dispersion interactions, Grimme's empirical dispersion correction GD3BJ was applied.[65]

RESULTS AND DISCUSSION

Three polystyrene samples, refer to Scheme 2, containing different end groups, namely TEMPO-PS (M_n = 3400 g mol^{-1} and $Đ$ = 1.2) and BU-PS$_{LM/HM}$ (M_n = 580 g mol^{-1} and $Đ$ = 1.01 and M_n = 3270 g mol^{-1} and $Đ$ = 1.03), have been selected to investigate the influence of the nature of the end group and the chain length on the gas phase structure of the PS ions. The choice of the polymer end-group is motivated by the fact that the TEMPO residue is anticipated to participate in the charge localization by catching a proton, unlike the butyl residue. Synthesized TEMPO-PS polymer has been fully characterized using NMR (refer to Figure S1) and MALDI-ToF experiments (refer to Figure S2), whereas the commercially available BU-PS$_{LM/HM}$ were only analyzed by MALDI-ToF (refer to Figures S3, S4, and S5).

Scheme 2. Chemical Structures of the Polystyrene Samples Used in the Present Investigation, TEMPO-PS: (M_n = 3400 g mol^{-1} and $Đ$ = 1.2) and BU-PS$_{LM/HM}$ (M_n = 580 g mol^{-1} and $Đ$ = 1.01 and M_n = 3270 g mol^{-1} and $Đ$ = 1.03)

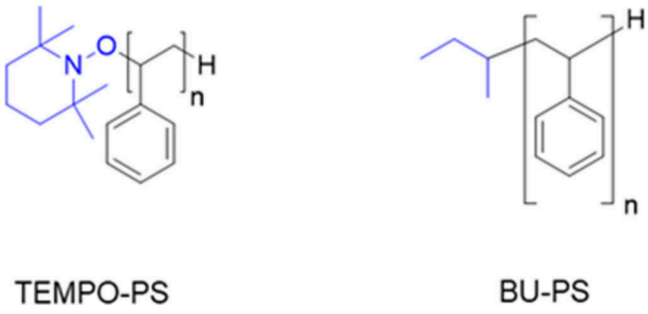

ESI-MS ANALYSIS OF PS

Polystyrene is best analyzed by mass spectrometry, either using MALDI or ESI, in the presence of Ag^+ ions because of favorable interactions between the π-electrons of the aromatic rings and the silver cations.[66]

Termination of the PS with the TEMPO group provides a basic site for protonation under positive ion ESI conditions and thus enables localization of at least one charge and even facilitates ionization without the addition of a cationization agent. The TEMPO-PS ESI-ToF mass spectrum is presented in Figure 1a and features a symmetrical peak distribution centered at m/z 1823 (DP 16), with the 104 u mass difference between two consecutive signals that is typical of singly charged (+1) PS ions. These ions are assigned to [TEMPO-PS + H]$^+$ ions based on the comparison between the isotope distribution with the theoretical one (refer to Figure S6). TEMPO-PS was further analyzed by ESI-ToF in the presence of $AgNO_3$ as a source of Ag^+ cationization agent in Figures 1b/ and S6. Besides the [TEMPO-PS + H]$^+$ ions, already detected in Figures 1a and S5, 2+ ions are detected for DP = 21−44 and are clearly ascribed as [TEMPO-PS + H + Ag]$^{2+}$ ions (refer to Figure S6 for the isotopic distribution analysis).

BU-PS$_{LM/HM}$ was also subjected to ESI-ToF analysis in the presence of $AgNO_3$ as the source of cationizing agent. As expected, no protonated BU-PS was detected due to the absence of a proton binding site unlike TEMPO. Nevertheless, as seen in Figure 1c and Figure S7, abundant singly and doubly charged ions are detected and correspond to [BU-PS$_{LM}$ + Ag]$^+$ and [BU-PS$_{HM}$ + 2Ag]$^{2+}$ ions, respectively. Note here that BU-PS$_{LM}$ mostly contains chains with DP = 3−13, whereas BU-PS$_{HM}$ contains chains with DP = 26−38. Again, the ion charge states and the ion compositions for both the 1+ and 2+ Bu-PS$_{LM/HM}$ ions have been established based on the comparison between the experimental isotopic distributions and simulated ones (refer to Figures S7 and S8).

IMS EXPERIMENTS ON GASEOUS TEMPO-PS AND BU-PS IONS

All PS ions, i.e., [TEMPO-PS + H]$^+$, [TEMPO-PS + H + Ag]$^{2+}$, [BU-PS$_{LM}$ + Ag]$^+$, and [BU-PS$_{HM}$ + 2Ag]$^{2+}$ ions, have been subjected to ion mobility experiments to investigate the influence of the nature of the end-group (TEMPO vs BU), of the chain length, of the charge state (1+ vs 2+), and of the

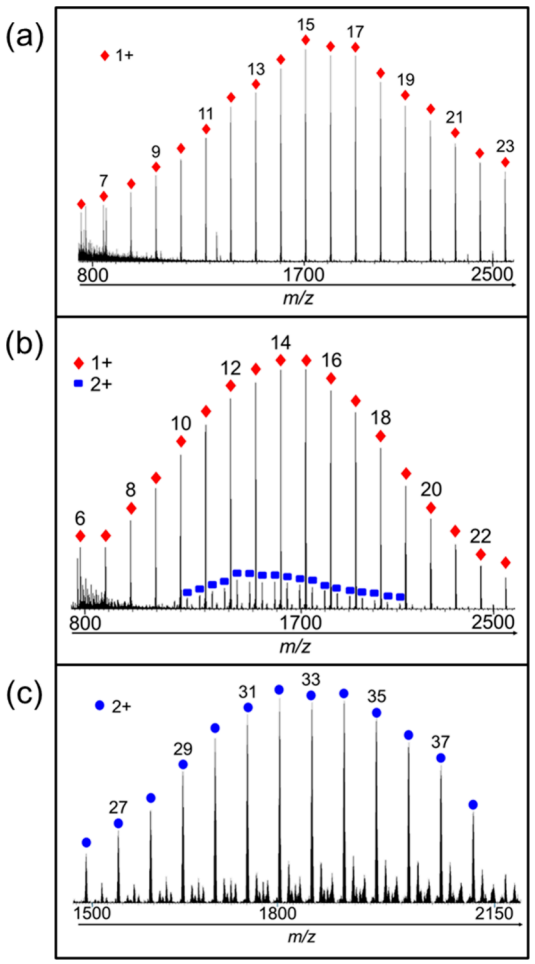

Figure 1. ESI-MS mass spectra of (a) TEMPO-PS (0.01 mg mL^{-1}) in acetonitrile/acetone 80/20, (b) TEMPO-PS (0.01 mg mL^{-1}) in acetonitrile/acetone 80/20 with $AgNO_3$ (0.0002 mg mL^{-1}), and (c) BU-PS_{HM} (0.01 mg mL^{-1}) in 80/20 acetonitrile/acetone with $AgNO_3$ (0.0002 mg mL^{-1}). Red ♦ correspond to $[TEMPO\text{-}PS + H]^+$, blue ■ represent the $[TEMPO\text{-}PS + H + Ag]^{2+}$, and blue ● correspond to $[BU\text{-}PS_{HM} + 2Ag]^{2+}$ ions. The numbers on the peaks correspond to the DP values of the corresponding ions.

cationizing agent (H^+ vs Ag^+) on the gas phase structure of the polymer ions.

This has been experimentally performed by (i) analyzing for all the ions the symmetry of the arrival time distribution (ATD), (ii) determining the ion CCS_{exp}, and (iii) monitoring the CCS_{exp} evolution over the mass range (DP = 6−23 for $[TEMPO\text{-}PS + H]^+$, DP = 21−44 for $[TEMPO\text{-}PS + H + Ag]^{2+}$, DP = 3−13 for $[BU\text{-}PS_{LM} + Ag]^+$, and DP = 26−38 for $[BU\text{-}PS_{HM} + 2Ag]^{2+}$). Asymmetrical ATD would reveal the presence of noninterconverting gas phase structures,[67] whereas plotting the CCS evolution as a function of mass (m/z), the so-called trend line analysis, enables (i) assessing the global 3D structure of the ions (sphere vs cylinder, for instance)[68,69] and (ii) detecting subtle modifications in the structure of macroions, typically the transition between extended and folded structures upon mass increase.[70] Charged polymer ions often adopt globular conformations in the gas phase, for which the evolution of CCS as a function of the mass is described by a power law, i.e., $CCS = A\,M^B$ where M is the molecular mass, B is ∼2/3 that of the characteristic value for a spherical evolution, and A is related to the ion density.[69] Polymer ions with B ∼ 2/3 are compact, with the spherical structure being considered as the densest arrangement, while ions with B > 2/3 are increasingly extended, with a value of B ∼ 1 characteristic of fully extended structures growing linearly with the number of monomer units (or the mass). On the basis of theoretical calculations, we recently demonstrated that extended objects such as helices have their B parameter tending to 1 as their mass (or length) tends to infinity, but at a different rate depending on the chemical nature of the side chains.[70,71]

Figures 2, S9, S10, and S11 contain the IMS data for $[TEMPO\text{-}PS + H]^+$, $[TEMPO\text{-}PS + H + Ag]^{2+}$, $[BU\text{-}PS_{LM} + Ag]^+$, and $[BU\text{-}PS_{HM} + 2\,Ag]^{2+}$ ions. As shown in Figures S9−S11, sharp and symmetrical arrival time distributions (ATD) have been recorded for all the 1+ and 2+ ions, indicating the presence of unique ion structures or structures that are interconverting very fast over the sampled mass ranges, as also confirmed by the quasi constant CCS resolution (R ∼ 40, that is the instrument resolution[72]) for all the analyzed ions (Figure S12). For TEMPO-PS ions, the CCS/mass evolutions for both the 1+ and 2+ ions are fitted by $CCS_{exp} = AM^B$, as shown in Figure 2a,b, with the B values determined at 0.69 and 0.70, respectively, indicating that the 3D structures cannot be considered as fully spherical (B = 2/3). Indeed, the B value is quite sensitive to the 3D structure, implying that slight differences in the B value could indicate strong modifications in the structures.[68] For example, we recently determined a B value at 0.72 for helical anionic peptoid ions (DP = 3−15).[69]

By approximating globular proteins as spheres, Ruotolo et al.[73] established that the ion density can be determined using eq 1 based on CCS trend line analysis. Doing so, i.e., by assuming that the PS ions were quasi spherical, we obtained ρ_{ccs} = 0.40 Da $Å^{-3}$ and 0.47 Da $Å^{-3}$ for the $[TEMPO\text{-}PS + H]^+$ and $[TEMPO\text{-}PS + H + Ag]^{2+}$ ions, respectively. On the basis of the reported density of bulk polystyrene, 0.96−1.05 g cm^{-3} say 0.57−0.62 Da $Å^{-3}$,[60] ρ_{ccs} are thus calculated by far lower for both the 1+ and 2+ ions. This indicates, in conjunction with the determined B parameters, that the 1+ and 2+ ions do not adopt spherical structures in the gas phase.

$$\rho_{ccs} = \frac{3}{4}\sqrt{\frac{\pi}{A^3}}\ (\mathrm{Da/Å^3}) \qquad (1)$$

Polyether and polyester polymer ions are characterized by the charge(s) positioned deep in the core of the ion structure with the flexible (and polar) polymer chain folded around the cationizing particle(s).[35] In the case of PS ions, we may imagine that silver ion stabilization by the phenyl rings also induces PS chain folding with the silver ion(s) incorporated within the globular ion. We thus analyzed $[BU\text{-}PS_{LM} + Ag]^+$ and $[BU\text{-}PS_{HM} + 2\,Ag]^{2+}$ ions, in which the butyl group is not participating in any cationization/protonation process. As shown in Figure 2c, d, the fitting process affords B = 0.81 and ρ_{ccs} = 1.43 Da $Å^{-3}$ (A = 0.95) and B = 0.68 and ρ_{ccs} = 0.33 Da $Å^{-3}$ (A = 2.48) for 1+ and 2+ BU-$PS_{LM/HM}$, respectively, values that clearly deviate from the bulk PS density.

MOLECULAR MODELING AND THEORETICAL CCS CALCULATION

Polystyrene Ion Shape Analysis. Atomistic simulations constitute an efficient approach to generating accurate information about the ion structure with a description at the atomistic level. CCS is used here to identify the best structure candidates among a set of generated ion geometries, upon

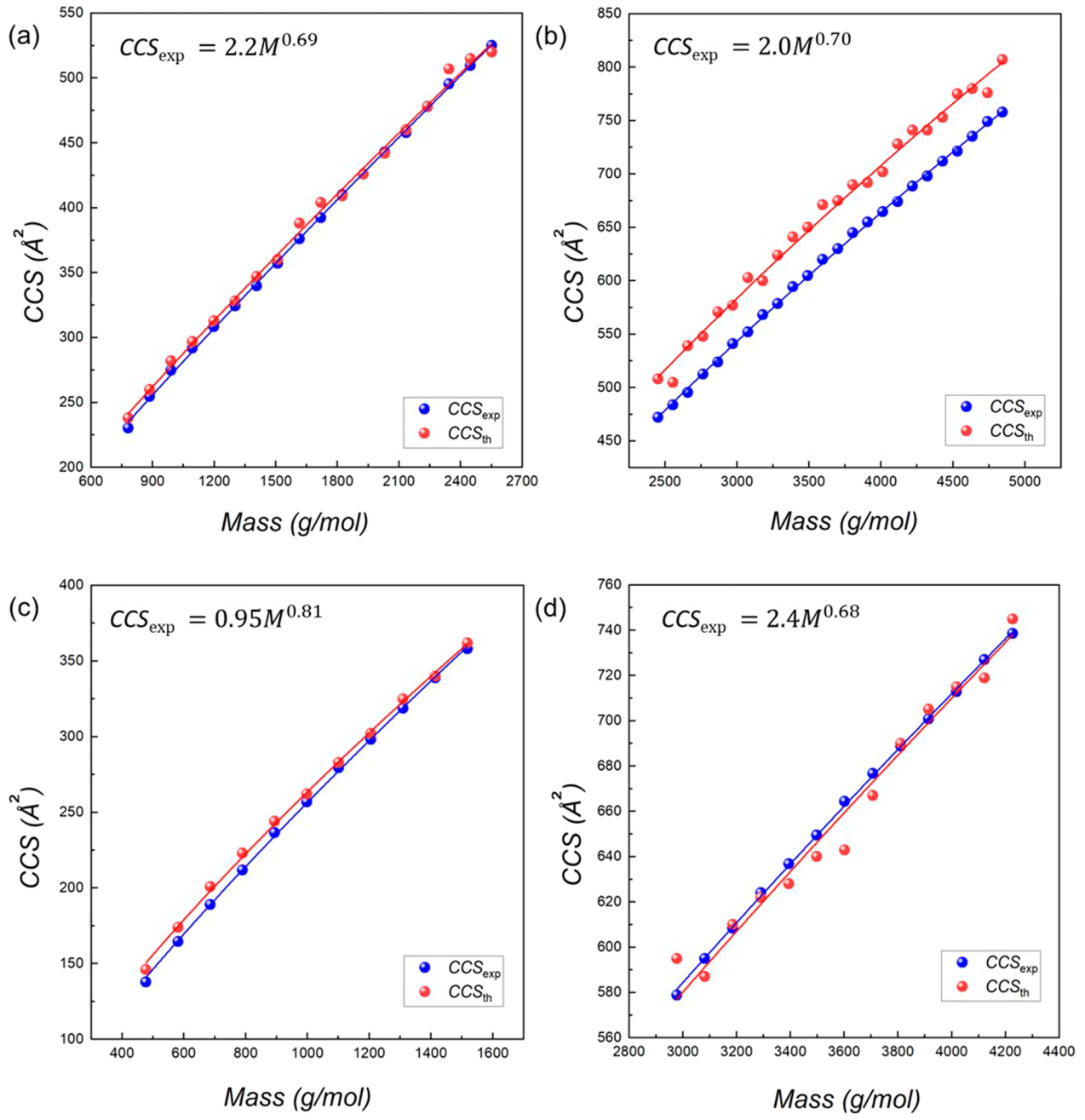

Figure 2. Ion mobility mass spectrometry analysis of TEMPO-PS and BU-$PS_{LM/HM}$: trend line analysis (CCS evolution with mass) of (a) $[TEMPO\text{-}PS + H]^+$, (b) $[TEMPO\text{-}PS + H + Ag]^{2+}$, (c) $[BU\text{-}PS_{LM} + Ag]^+$, and (d) $[BU\text{-}PS_{HM} + 2Ag]^{2+}$. The blue curves and fitting equations correspond to the experimental CCS evolutions. The red curves correspond to theoretical (MD) CCS evolutions.

direct comparison between the CCS_{exp} and CCS_{th}.[74] Using molecular dynamics simulations, we optimized the structures of all gaseous 1+ and 2+ PS ions detected in the ESI experiments. In the case of the protonated polymers, we first used DFT calculations to establish the preferential position of the added proton on the TEMPO end group. As shown in Figure S13, *N*-protonation is favored over *O*-protonation, with a stabilization energy of ~32 kcal mol^{-1}.

CCS_{th} were calculated from the atomistic simulations using the trajectory method implemented in Collisdoscope[62] and then compared with the CCS_{exp} in Figure 2. For $[TEMPO\text{-}PS + H]^+$, $[BU\text{-}PS_{LM} + Ag]^+$, and $[BU\text{-}PS_{HM} + 2\ Ag]^{2+}$ ions, the CCS_{th} values are in very good agreement with the experimental ones, whereas in the case of $[TEMPO\text{-}PS + H + Ag]^{2+}$ ions, the CCS_{th} values are consistently overestimated by ~9% compared to the experimental ones.[62] Since the CCS_{th} curve is parallel to the CCS_{exp} evolution for the $[TEMPO\text{-}PS + H + Ag]^{2+}$ ions, there is most likely a systematic error made theoretically for these systems. For dications, a parameter that is not accounted for by our calculations is the screening of Coulomb repulsion between the two cations by the intervening medium. The description of such a screening would require exploring the use of more complex polarizable force fields, which is beyond the scope of the present work. The screening effects are expected to condense further the ions and be more pronounced when there is a large separation between the ions (i.e., a wider polarizable medium). This is actually the case for the $[TEMPO\text{-}PS + H + Ag]^2$ compared to the $[BU\text{-}PS_{HM} + 2$

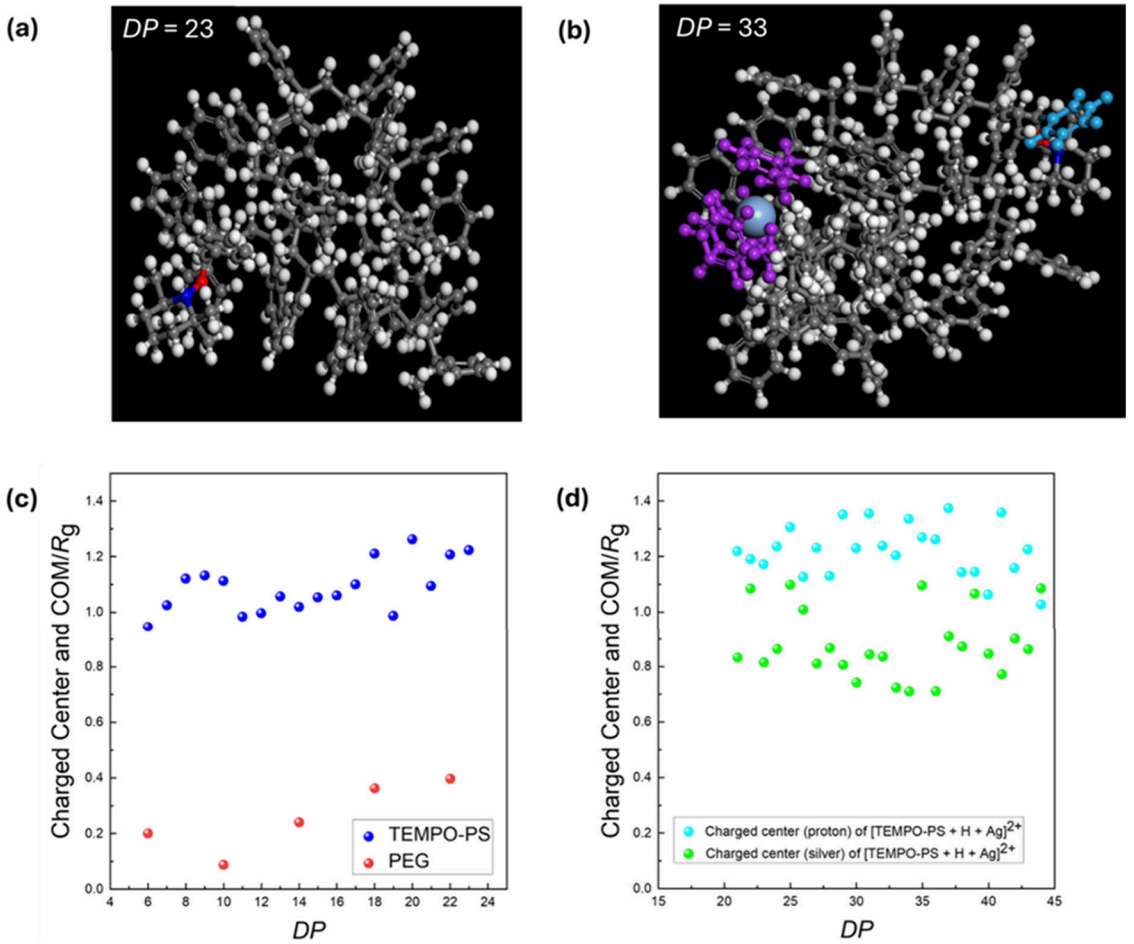

Figure 3. Molecular dynamics simulations (PCFF force field, 300 K, 25 ns) of TEMPO-PS ions: (a) snapshot of the last frame of the MD for $[TEMPO\text{-}PS + H]^+$ (DP = 23) and (b) snapshot of the last frame of the MD for $[TEMPO\text{-}PS + H + Ag]^{2+}$ (DP = 33). The colored styrene rings are involved in the cation-π interaction; (c) evolution of the distance between the charged center (H^+ or Na^+) and the center-of-mass (COM) normalized by the ion radius of gyration (R_g) for $[TEMPO\text{-}PS + H]^+$ (blue dots) and $[PEG + Na]^+$ (red dots) (PEG stands for polyethylene glycol, see Figure S14 for the optimized ion structure); (d) evolution of the distance between the H^+ (cyan dots) and Ag^+ (green dots) and the center-of-mass (COM) normalized by the ion radius of gyration (R_g) for $[TEMPO\text{-}PS + H + Ag]^{2+}$. Refer also Figure S15 for the evolution of the intercharge distance for $[TEMPO\text{-}PS + H + Ag]^{2+}$ ions.

$Ag]^{2+}$ ions (see Figures S15 and S16), in line with the fact that the cross sections are overestimated for the former ions.

Figure 3 shows the optimized structures of $[TEMPO\text{-}PS + H]^+$ (DP = 23) and $[TEMPO\text{-}PS + H + Ag]^{2+}$ (DP = 33), as typical examples selected for the 1+ and 2+ series of ions. We observe that both the 1+ and 2+ ions appear as compact structures with the protonated TEMPO end group located on the edge of the folded chain. For the 1+ ions, this is clearly different from the situation encountered with a classical (traditional) polymer such as Na^+-cationized polyethers and polyesters, where the Na^+ ion is stabilized deeply into the core of the globular structure,[35] see Figure S14 for a typical polyethylene glycol (PEG) ion. To illustrate this particularity, the distance between the charged center (protonated TEMPO or Na^+) and the center-of-mass of the ion for, respectively, $[TEMPO\text{-}PS + H]^+$ or $[PEG + Na]^+$ ions, has been divided by the radius of gyration (R_g) of the ion to generate normalized data for increasing DP. As shown in Figure 3c, the normalized distance is between 0.1 and 0.4 for the $[PEG + Na]^+$ ions but increases up to ~1 for the $[TEMPO\text{-}PS + H]^+$ ions, implying that the charged end group clearly remains at the surface of the ion structure over the investigated DP range. As shown in Figure 3b for the $[TEMPO\text{-}PS + H + Ag]^{2+}$ ions, the protonated TEMPO remains on the surface of the ion and the added Ag^+ cation is located at a diametrically opposite position (Figure 3d), although also at the surface of the ion. The H^+/Ag^+ distance remains nearly constant around 15−20 Å over the whole investigated DP range (that extends from DP = 21 to 44) to minimize the electrostatic repulsion between both charged centers (see Figure S15). Again these $[TEMPO\text{-}PS + H + Ag]^{2+}$ ions appear as compact structures. In a recent study related to gas phase dendrimer ions,[68] the so-called solvent-accessible surface area (SASA) has been introduced to estimate the effective ion density to be compared to the CCS-determined density (ρ_{ccs}).[75] SASA corresponds to the total area of the ion envelope, and in our simulations, helium is considered as the probing atom (see the Experimental Section). The respective molecular volume (V_{SASA}) can subsequently be used to determine the ion effective density, namely ρ_{SASA}, that is only equal to ρ_{ccs} for hard spheres.[68] We determined the SASA for all the $[TEMPO\text{-}PS + H]^+$ and $[TEMPO\text{-}PS+ H + Ag]^{2+}$ ions, see Tables S3 and S4, and calculated an average $\langle\rho_{SASA}\rangle$ = 0.62 Da $Å^{-3}$ and 0.65 Da $Å^{-3}$ for the 1+ and 2+ ions, respectively. These calculated effective densities (0.62−0.65 Da $Å^{-3}$) lie close to the bulk PS density (0.57−0.62 Da $Å^{-3}$),[60] revealing that the ion folding ends up

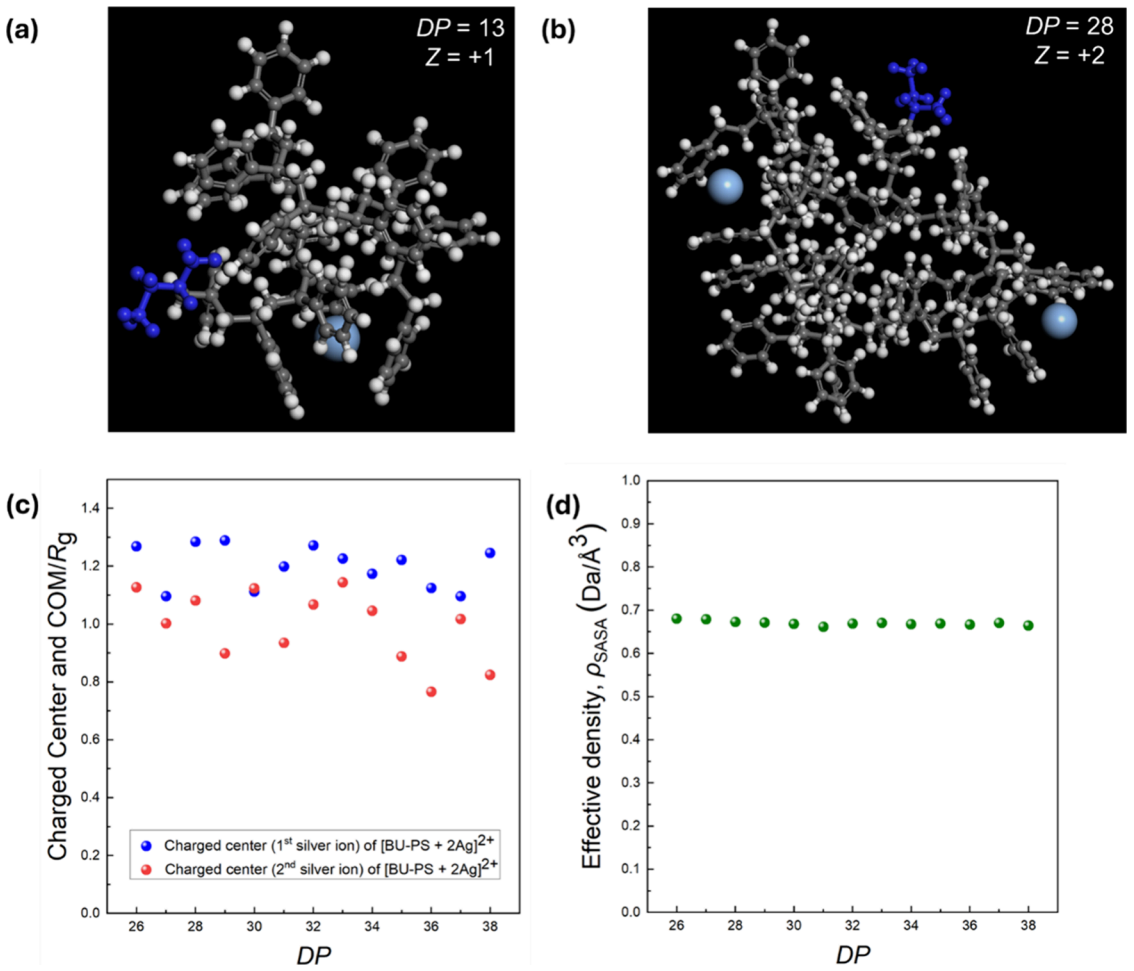

Figure 4. Molecular dynamics simulations (PCFF force field, 300 K, 25 ns) of BU-PS ions: (a) snapshot of the last frame of the MD for $[\text{Bu-PS}_{\text{LM}} + \text{Ag}]^+$ (DP = 13); (b) snapshot of the last frame of the MD for $[\text{BU-PS}_{\text{HM}} + 2\text{Ag}]^{2+}$ (DP = 28); (c) evolution of the distances between the charged centers (Ag^+ ions) and the center-of-mass (COM) normalized by the ion radius of gyration (R_g) for $[\text{BU-PS} + 2\text{Ag}]^{2+}$; blue and red ● correspond to both silver ions; and (d) evolution of the effective density, ρ_{SASA}, from DP = 26 to DP = 38 for $[\text{BU-PS}_{\text{HM}} + 2\text{Ag}]^{2+}$. Refer also Figure S16 for the evolution of the intercharge distance for $[\text{BU-PS}_{\text{HM}} + 2\text{Ag}]^{2+}$ ions.

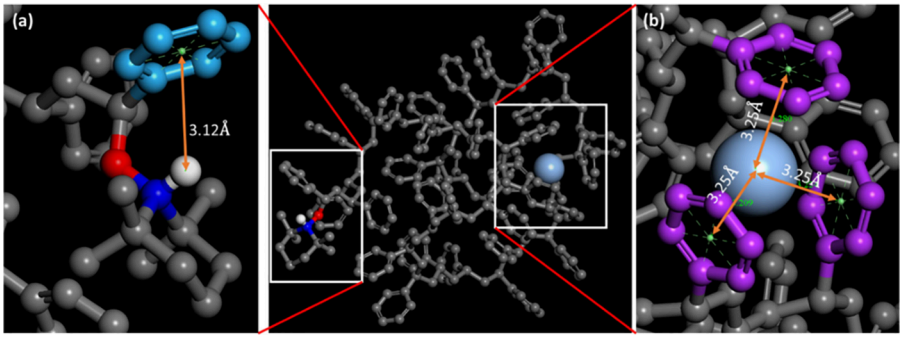

Figure 5. Molecular dynamics simulations (PCFF force field, 300 K, 25 ns) of $[\text{TEMPO-PS} + \text{H} + \text{Ag}]^{2+}$ ions (DP = 33). Snapshot of the last frame of the MD with enlarged views of the charged centers: (a) proton-π interaction around the TEMPO end group and (b) cation-π interaction involving the Ag^+ ion and three phenyl rings of the PS backbone.

with dense PS ions, whose high density is mainly caused by the PS chain compaction.

Similar results have been obtained when examining the optimized geometries of $[\text{Bu-PS}_{\text{LM}} + \text{Ag}]^+$ and $[\text{BU-PS}_{\text{HM}} + 2\text{Ag}]^{2+}$ ions, as shown in Figure 4 and gathered in Tables S5 and S6. Indeed, for the 1+ ions (DP = 13), the Ag^+ cation remains at the surface of the globular ions, while for the 2+ ions, both Ag^+ ions are diametrically positioned at the surface of the globular ion with a quasi-constant distance of ∼15 Å from DP 26 to 38 (see Figure S16) and an effective density staying constant at 0.65 Da $Å^{-3}$ (Figure 4d). All the detected ions can therefore be considered as highly compact and fully folded structures.

Globally, a globular ion with an egglike shape represents the best structure to account for the experimental and theoretical data that can be summarized as follows: (i) regardless of the

charge state and the chain ends, the PS chain folds into the most compact structure with a constant effective density (ρ_{SASA}) close to the bulk PS density; (ii) the charge(s) is (are) excluded from the PS core and remain(s) at the surface of the globular ions; and (iii) the intercharge distance in 2+ ions remains constant ~15−20 Å over the entire investigated DP range for both Ag^+/H^+ (see Figure S15) and Ag^+/Ag^+ pairs (see Figure S16).

Polystyrene Ion Molecular Structure Analysis. In addition to establishing the global shape of the ions, MD simulations also allow analyzing the ion structure at the atomistic level by examining the intramolecular interactions responsible for the chain folding.

As featured in Figure 5, protonated TEMPO is stabilized by a cation (H^+)-π interaction involving only the first styrene residue, with a proton-phenyl ring distance at ~3.1 Å whatever the charge state of the polymer ion. On the other hand, the silver ions (1+ and 2+ ions) are strongly interacting with three phenyl rings in a cage arrangement with distances around 3.25 Å between Ag^+ and the geometrical center of the phenyl rings.[66,76] With the use of DFT calculations, we optimized the geometry of a model complex, associating three benzene molecules to a single Ag^+ cation. As shown in Figure S17, in the optimized geometry, the silver cation is located in the center of the benzene triad with cation-benzene distances around 2.9 Å, thus corroborating our MD calculations.

Another aspect to be discussed is the spatial arrangement of the PS backbone within the globular ions or, in other words, the determination of whether there is a preferred three-dimensional folding for the polymer chain. We examined the folding of the polymer backbone within the optimized $[BU\text{-}PS + 2\ Ag]^{2+}$ ions whose CCS_{th} are reported in Figure 2c. As sketched in Figure 6, we identified two different scaffolds that

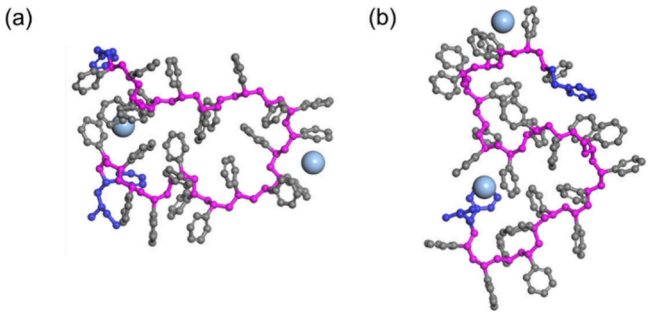

Figure 6. Molecular dynamics simulations (PCFF force field, 300 K, 25 ns) of $[BU\text{-}PS + 2\ Ag]^{2+}$ ions (DP = 26): snapshots of the last frame of the MD featuring U-shape and S-shape folding for the PS backbone. As described in the main text, these two geometries have been obtained from different input geometries presented in Figure S18. Here, blue is used to indicate the end groups and pink for the polymer backbone: (a) "U" shape structure for $[BU\text{-}PS + Ag]^{2+}$ ions (DP = 26) and (b) "S" shape structure for $[BU\text{-}PS + 2Ag]^{2+}$ ions (DP = 26).

are described as U-folding and S-folding in the following discussion. The U-folding terminology reflects that the polymer backbone adopts a looplike structure with one silver cation lying around in the middle of the chain and the second one associating the two extremities of the linear polymer; see Figure 6a. The S-folding is characterized by a spatial arrangement with two loops and one Ag+ cation at each extremity of the backbone; see Figure 6b. Both scaffolds are randomly observed over the entire DP range without any trend, implying that the chain randomly folds during the MD simulations.

As for a typical example, in Figure 6, U-folding and S-folding are generated by MD simulations from two different input structures for DP = 26 (see Figure S18 for the input structures). Moreover, these ions, both characterized by CCS_{th} = 584/585 $Å^2$, are not experimentally distinguishable and are likely to coexist in the gas phase.

Polystyrene Ion vs Polyether Ion Folding in the Gas Phase: What Is the Role of the Charge? There is thus an intrinsic difference between the gas phase structures of $[PS + Ag]^+$ ions and $[PEG + Na]^+$ ions since the Na^+ ion is located close to the center of mass of the globular ions (Figures 3c and S14), whereas the Ag^+ ion (or protonated TEMPO) remains mostly at the surface of the globular ions. For the $BU\text{-}PS_{LM/HM}$ 1+ and 2+ ions, we also noticed that the butyl end-group is invariably excluded from the PS core of the globular ions, see Figure 4 for typical examples. To understand the folding mechanism of $[BU\text{-}PS + Ag]^+$ ions, we performed 36 MD simulations starting from three different linear input structures for DP = 44, i.e., with the Ag^+ positioned close to the butyl end group, near the middle of the chain, and close to the hydrogen atom end-group, see Figure S19. In order to obtain a statistically relevant folding mechanism, each input geometry was submitted to 12 independent MD runs to generate 12 independent equilibrated geometries. We then evaluated the relative position of the Ag^+ in the equilibrated structures by calculating the distance between the charged center and the center-of-mass normalized by the radius of gyration (R_g), see Table S7. We noticed (i) that the Ag^+ ion does not diffuse along the polymeric chain (see also Figure 7); and (ii) that, in all folded structures, the Ag^+ ion is stabilized at the surface of the coiled chain, as the ratio between the charged/center-of-mass distance normalized by the radius of gyration is systematically around 0.7 and 0.8. The same methodology has been applied to the case of the $[PEG + Na]^+$ ion (DP = 44) folding, starting from two initial uncoiled states where the Na^+ ion was placed near the beginning and into the middle of the polymeric chain (Figure S20). Regardless of the initial geometry, all MD simulations ended up with coiled chains where the sodium cation is stabilized at the core of the polyether globule at an average position (distance between the sodium ion and the center-of-mass (COM) normalized by the ion radius of gyration) of ~0.4, see Table S7.

When there are frame-by-frame MD trajectories for both the $[BU\text{-}PS + Ag]^+$ and $[PEG + Na]^+$ ions (DP = 44), we realized that the folding mechanisms are intrinsically different for both families of ions. In the case of PS ions, as illustrated in Figure 7, the charge does not participate in the folding process, and coiling is initiated by the phenyl ring interaction in the middle of the chain on the way to the PS-only core, from which the butyl end group and the silver ion are excluded, leading to the final compaction of the ions. In Figures S21 and S22, similar behaviors were detected during the MD starting from the input geometries presenting the Ag^+ ion in the middle or at the other extremity of the PS backbone, revealing that the ion folding is mostly driven by $\pi-\pi$ interactions rather than by charge stabilization.

On the other hand, for the $[PEG + Na]^+$ ions, see Figure 8, the folding of the chain is triggered by the stabilization of the Na^+ ion by the basic O sites present all along the flexible polymer chain, whereas the absence of acidic sites on the chain

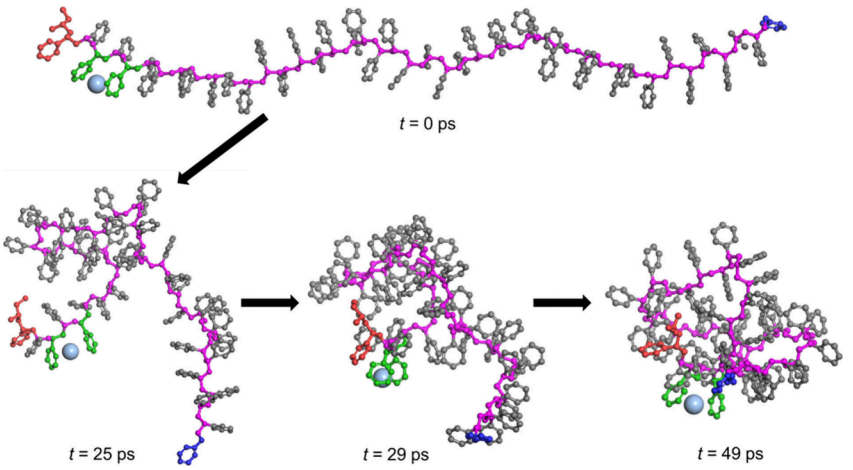

Figure 7. Molecular dynamics simulations (PCFF force field, 300 K, 2 ns) of $[BU\text{-}PS + Ag]^+$ ions (DP = 44) with the Ag^+ ion initially positioned close to the butyl end-group of the PS backbone (PS_{BU}): snapshots at different times of the trajectory revealing that the folding process is mostly initiated by $\pi-\pi$ interactions between phenyl rings with the charge and the butyl end group remaining at the surface of the equilibrated structure. The styrene residues highlighted in green pinpoint the initial and final positions of the Ag^+ ion.

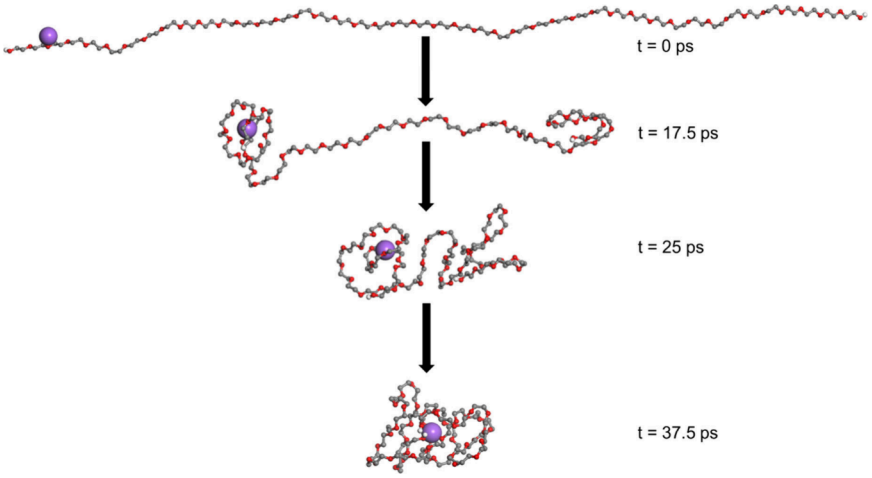

Figure 8. Molecular dynamics simulations (PCFF force field, 300 K, 2 ns) of $[PEG + Na]^+$ ions (DP = 44) with the Na^+ ion initially positioned close to the extremity of the PEG backbone: snapshots at different points of the trajectory revealing that the folding process is mostly initiated by Na^+-dipole interactions between the oxygen atoms and the charge, generating globular ions with the Na^+ ion deeply settled in the PEG core; here, position of the Na^+ ion at the end of dynamics does not depend on the position of the Na^+ ion in the input structure.

prevents any intramolecular folding. When the cation is fully stabilized by the polyether chain, the rest of the polyether chain progressively collapses around the initial nucleus to generate a dense globular structure with the Na^+ ion settled deep in the core of the ion. Such behavior is also allowed by the greater flexibility of the PEG chain compared to the PS backbone.

CONCLUSIONS

A combination between IMS-MS and molecular dynamics simulations has been used to investigate the structure of polymer ions constituted by rigid and apolar monomer units, i.e., styrene residues, and hydrophilic/hydrophobic end groups, i.e., TEMPO and butyl end-groups. Experimental and theoretical CCS were determined to establish the 3D shape of the 1+ and 2+ PS ions. Trend line analyses (CCS versus mass plots) have been shown to be inefficient in predicting the exact shape of the ions. Experimental CCS became much more structure informative when compared with theoretical data generated using molecular dynamics simulations at the atomistic level of the ion structure. By computing the solvent accessible surface area (SASA), we initially established that the PS backbone is densely packed within elliptic-shaped ions with an effective density close to the bulk PS density. We further established that the charges (1+ and 2+ ions) are systematically positioned close to the surface of the folded ions, at variance with polyether ions in which the sodium ions are settled deep in the core of the ion structure. We also demonstrated by performing MD simulations starting from different input structures that the PS backbone can fold in different structures, generating U- and S-shapes, possessing quasi-identical theoretical CCS that cannot be distinguished by experiment. Such a behavior is reminiscent of solution phase processes, where random coils are often involved to account for the hydrodynamic volumes of floppy polymers. Finally, to account for the intrinsic differences between the PS and the PEG ions, we used MD simulations to demonstrate that the folding of the PS rigid chain is induced by phenyl ring interactions with the charge ultimately remaining excluded from the core of the globular ions, whereas the folding of

polyether ions is initiated by the folding of the flexible polyether chain around the sodium ion that remains deeply settled in the core of the ions. Critically, compared to literature results, our data reveal that in large PS structures charges, typically the silver cations, are not merely sandwiched between two phenyl rings but ligated in 3-dimensions inducing the overall collapse of the tertiary structure.

AUTHOR INFORMATION

Corresponding Author

Pascal Gerbaux − *Organic Synthesis and Mass Spectrometry Laboratory, Center of Innovation and Research in Materials and Polymers (CIRMAP), University of Mons - UMONS, B-7000 Mons, Belgium;* orcid.org/0000-0001-5114-4352; Email: pascal.gerbaux@umons.ac.be

Authors

Sarajit Naskar − *Organic Synthesis and Mass Spectrometry Laboratory, Center of Innovation and Research in Materials and Polymers (CIRMAP) and Laboratory for Chemistry of Novel Materials, Center of Innovation and Research in Materials and Polymers (CIRMAP), University of Mons - UMONS, B-7000 Mons, Belgium; Center for Materials Science, School of Chemistry and Physics, Queensland University of Technology (QUT), Brisbane, Queensland 4000, Australia*

Andrea Minoia − *Laboratory for Chemistry of Novel Materials, Center of Innovation and Research in Materials and Polymers (CIRMAP), University of Mons - UMONS, B-7000 Mons, Belgium*

Quentin Duez − *Organic Synthesis and Mass Spectrometry Laboratory, Center of Innovation and Research in Materials and Polymers (CIRMAP), University of Mons - UMONS, B-7000 Mons, Belgium;* orcid.org/0000-0002-9067-7917

Aidan Izuagbe − *Center for Materials Science, School of Chemistry and Physics, Queensland University of Technology (QUT), Brisbane, Queensland 4000, Australia*

Julien De Winter − *Organic Synthesis and Mass Spectrometry Laboratory, Center of Innovation and Research in Materials and Polymers (CIRMAP), University of Mons - UMONS, B-7000 Mons, Belgium;* orcid.org/0000-0003-3429-5911

Stephen J. Blanksby − *Center for Materials Science, School of Chemistry and Physics, Queensland University of Technology (QUT), Brisbane, Queensland 4000, Australia;* orcid.org/0000-0002-8560-756X

Christopher Barner-Kowollik − *Center for Materials Science, School of Chemistry and Physics, Queensland University of Technology (QUT), Brisbane, Queensland 4000, Australia;* orcid.org/0000-0002-6745-0570

Jérôme Cornil − *Laboratory for Chemistry of Novel Materials, Center of Innovation and Research in Materials and Polymers (CIRMAP), University of Mons - UMONS, B-7000 Mons, Belgium;* orcid.org/0000-0002-5479-4227

Notes

The authors declare no competing financial interest.

ACKNOWLEDGMENTS

The S^2MOs lab is grateful to the "Fonds National de la Recherche Scientifique (FRS-FNRS)" for financial support for the acquisition of the Waters Synapt G2-Si mass spectrometer. S.N. thanks UMONS and QUT for his Ph.D. thesis grant. Computational resources have been provided by the Consortium des Équipements de Calcul Intensif (CÉCI), funded by the Fonds de la Recherche Scientifique de Belgique (F.R.S.-FNRS) under Grant no. 2.5020.11 and by the Walloon Region (ZENOBE and LUCIA Tier-1 supercomputers). Q.D. and J.C. are FNRS research fellows. C.B.-K. and S.B. acknowledge continued support from the Queensland University of Technology (QUT) and its Centre for Materials Science.

REFERENCES

(1) Steinkoenig, J.; Cecchini, M. M.; Reale, S.; Goldmann, A. S.; Barner-Kowollik, C. Supercharging Synthetic Polymers: Mass Spectrometric Access to Nonpolar Synthetic Polymers. *Macromolecules* **2017**, *50* (20), 8033−8041.

(2) Karas, M.; Bachmann, D.; Bahr, U.; Hillenkamp, F. Matrix-Assisted Ultraviolet Laser Desorption of Non-Volatile Compounds. *International Journal of Mass Spectrometry and Ion Processes* **1987**, *78*, 53−68.

(3) Karas, M.; Hillenkamp, F. Laser Desorption Ionization of Proteins with Molecular Masses Exceeding 10,000 Da. *Anal. Chem.* **1988**, *60* (20), 2299−2301.

(4) Van Berkel, W. J. H.; Van Den Heuvel, R. H. H.; Versluis, C.; Heck, A. J. R. Detection of Intact megaDalton Protein Assemblies of Vanillyl-alcohol Oxidase by Mass Spectrometry. *Protein Sci.* **2000**, *9* (3), 435−439.

(5) Hanton, S. D. Mass Spectrometry of Polymers and Polymer Surfaces. *Chem. Rev.* **2001**, *101* (2), 527−570.

(6) De Bruycker, K.; Welle, A.; Hirth, S.; Blanksby, S. J.; Barner-Kowollik, C. Mass Spectrometry as a Tool to Advance Polymer Science. *Nat. Rev. Chem.* **2020**, *4* (5), 257−268.

(7) Montaudo, M. S. Mass Spectra of Copolymers. *Mass Spectrom. Rev.* **2002**, *21* (2), 108−144.

(8) Wesdemiotis, C.; Williams-Pavlantos, K. N.; Keating, A. R.; McGee, A. S.; Bochenek, C. Mass Spectrometry of Polymers: A Tutorial Review. *Mass Spectrom. Rev.* **2024**, *43*, 427−476.

(9) Crecelius, A. C.; Becer, C. R.; Knop, K.; Schubert, U. S. Block Length Determination of the Block Copolymer mPEG- *b* -PS Using MALDI-TOF MS/MS. *J. Polym. Sci. A Polym. Chem.* **2010**, *48* (20), 4375−4384.

(10) Weidner, S. M.; Trimpin, S. Mass Spectrometry of Synthetic Polymers. *Anal. Chem.* **2010**, *82* (12), 4811−4829.

(11) Crotty, S.; Gerişlioğlu, S.; Endres, K. J.; Wesdemiotis, C.; Schubert, U. S. Polymer Architectures via Mass Spectrometry and Hyphenated Techniques: A Review. *Anal. Chim. Acta* **2016**, *932*, 1−21.

(12) Charles, L.; Chendo, C.; Poyer, S. Ion Mobility Spectrometry–Mass Spectrometry Coupling for Synthetic Polymers. *Rapid Commun. Mass Spectrom.* **2020**, *34* (S2), No. e8624.
(13) Jackson, A. T.; Scrivens, J. H.; Williams, J. P.; Baker, E. S.; Gidden, J.; Bowers, M. T. Microstructural and Conformational Studies of Polyether Copolymers. *Int. J. Mass Spectrom.* **2004**, *238* (3), 287–297.
(14) McEwen, C. N.; Peacock, P. M. Mass Spectrometry of Chemical Polymers. *Anal. Chem.* **2002**, *74* (12), 2743–2748.
(15) Weidner, S. M.; Trimpin, S. Mass Spectrometry of Synthetic Polymers. *Anal. Chem.* **2008**, *80* (12), 4349–4361.
(16) Ito, K.; Kitagawa, S.; Ohtani, H. Analysis of Multiply Charged Poly(Ethylene Oxide-Co-Propylene Oxide) Using Electrospray Ionization-Ion Mobility Spectrometry-Mass Spectrometry. *ANAL. SCI.* **2019**, *35* (2), 169–174.
(17) Austin, C. A.; Inutan, E. D.; Bohrer, B. C.; Li, J.; Fischer, J. L.; Wijerathne, K.; Foley, C. D.; Lietz, C. B.; Woodall, D. W.; Imperial, L. F.; Clemmer, D. E.; Trimpin, S.; Larsen, B. S. Resolving Isomers of Star-Branched Poly(Ethylene Glycols) by IMS-MS Using Multiply Charged Ions. *J. Am. Soc. Mass Spectrom.* **2021**, *32* (1), 21–32.
(18) Hoskins, J. N.; Trimpin, S.; Grayson, S. M. Architectural Differentiation of Linear and Cyclic Polymeric Isomers by Ion Mobility Spectrometry-Mass Spectrometry. *Macromolecules* **2011**, *44* (17), 6915–6918.
(19) Foley, C. D.; Zhang, B.; Alb, A. M.; Trimpin, S.; Grayson, S. M. Use of Ion Mobility Spectrometry–Mass Spectrometry to Elucidate Architectural Dispersity within Star Polymers. *ACS Macro Lett.* **2015**, *4* (7), 778–782.
(20) Morsa, D.; Defize, T.; Dehareng, D.; Jérôme, C.; De Pauw, E. Polymer Topology Revealed by Ion Mobility Coupled with Mass Spectrometry. *Anal. Chem.* **2014**, *86* (19), 9693–9700.
(21) Liénard, R.; Duez, Q.; Grayson, S. M.; Gerbaux, P.; Coulembier, O.; De Winter, J. Limitations of Ion Mobility Spectrometry-mass Spectrometry for the Relative Quantification of Architectural Isomeric Polymers: A Case Study. *Rapid Commun. Mass Spectrom.* **2020**, *34* (S2), No. e8660.
(22) Trimpin, S.; Clemmer, D. E. Ion Mobility Spectrometry/Mass Spectrometry Snapshots for Assessing the Molecular Compositions of Complex Polymeric Systems. *Anal. Chem.* **2008**, *80* (23), 9073–9083.
(23) Tintaru, A.; Chendo, C.; Wang, Q.; Viel, S.; Quéléver, G.; Peng, L.; Posocco, P.; Pricl, S.; Charles, L. Conformational Sensitivity of Conjugated Poly(Ethylene Oxide)-Poly(Amidoamine) Molecules to Cations Adducted upon Electrospray Ionization–A Mass Spectrometry, Ion Mobility and Molecular Modeling Study. *Anal. Chim. Acta* **2014**, *808*, 163–174.
(24) Snyder, S. R.; Wesdemiotis, C. Elucidation of Low Molecular Weight Polymers in Vehicular Engine Deposits by Multidimensional Mass Spectrometry. *Energy Fuels* **2021**, *35* (2), 1691–1700.
(25) Duez, Q.; Moins, S.; Coulembier, O.; De Winter, J.; Cornil, J.; Gerbaux, P. Assessing the Structural Heterogeneity of Isomeric Homo and Copolymers: An Approach Combining Ion Mobility Mass Spectrometry and Molecular Dynamics Simulations. *J. Am. Soc. Mass Spectrom.* **2020**, *31* (11), 2379–2388.
(26) Baker, E. S.; Gidden, J.; Simonsick, W. J.; Grady, M. C.; Bowers, M. T. Sequence Dependent Conformations of Glycidyl Methacrylate/Butyl Methacrylate Copolymers in the Gas Phase. *Int. J. Mass Spectrom.* **2004**, *238* (3), 279–286.
(27) Amalian, J.-A.; Cavallo, G.; Al Ouahabi, A.; Lutz, J.-F.; Charles, L. Revealing Data Encrypted in Sequence-Controlled Poly(Alkoxyamine Phosphodiester)s by Combining Ion Mobility with Tandem Mass Spectrometry. *Anal. Chem.* **2019**, *91* (11), 7266–7272.
(28) Lanucara, F.; Holman, S. W.; Gray, C. J.; Eyers, C. E. The Power of Ion Mobility-Mass Spectrometry for Structural Characterization and the Study of Conformational Dynamics. *Nature Chem.* **2014**, *6* (4), 281–294.
(29) De Winter, J.; Lemaur, V.; Ballivian, R.; Chirot, F.; Coulembier, O.; Antoine, R.; Lemoine, J.; Cornil, J.; Dubois, P.; Dugourd, P.; Gerbaux, P. Size Dependence of the Folding of Multiply Charged Sodium Cationized Polylactides Revealed by Ion Mobility Mass Spectrometry and Molecular Modelling. *Chem.—Eur. J.* **2011**, *17* (35), 9738–9745.
(30) Smith, D. P.; Knapman, T. W.; Campuzano, I.; Malham, R. W.; Berryman, J. T.; Radford, S. E.; Ashcroft, A. E. Deciphering Drift Time Measurements from Travelling Wave Ion Mobility Spectrometry-Mass Spectrometry Studies. *Eur. J. Mass Spectrom (Chichester)* **2009**, *15* (2), 113–130.
(31) Haler, J. R. N.; Far, J.; Aqil, A.; Claereboudt, J.; Tomczyk, N.; Giles, K.; Jérôme, C.; De Pauw, E. Multiple Gas-Phase Conformations of a Synthetic Linear Poly(Acrylamide) Polymer Observed Using Ion Mobility-Mass Spectrometry. *J. Am. Soc. Mass Spectrom.* **2017**, *28* (11), 2492–2499.
(32) Haler, J. R. N.; Lemaur, V.; Far, J.; Kune, C.; Gerbaux, P.; Cornil, J.; De Pauw, E. Sodium Coordination and Protonation of Poly(Ethoxy Phosphate) Chains in the Gas Phase Probed by Ion Mobility-Mass Spectrometry. *J. Am. Soc. Mass Spectrom.* **2020**, *31* (3), 633–641.
(33) Haler, J. R. N.; Far, J.; De La Rosa, V. R.; Kune, C.; Hoogenboom, R.; De Pauw, E. Using Ion Mobility–Mass Spectrometry to Extract Physicochemical Enthalpic and Entropic Contributions from Synthetic Polymers. *J. Am. Soc. Mass Spectrom.* **2021**, *32* (1), 330–339.
(34) Haler, J. R. N.; Béchet, E.; Kune, C.; Far, J.; De Pauw, E. Geometric Analysis of Shapes in Ion Mobility–Mass Spectrometry. *J. Am. Soc. Mass Spectrom.* **2022**, *33* (2), 273–283.
(35) Gidden, J.; Wyttenbach, T.; Jackson, A. T.; Scrivens, J. H.; Bowers, M. T. Gas-Phase Conformations of Synthetic Polymers: Poly(Ethylene Glycol), Poly(Propylene Glycol), and Poly(Tetramethylene Glycol). *J. Am. Chem. Soc.* **2000**, *122* (19), 4692–4699.
(36) Gidden, J.; Jackson, A. T.; Scrivens, J. H.; Bowers, M. T. Gas Phase Conformations of Synthetic Polymers: Poly (Methyl Methacrylate) Oligomers Cationized by Sodium Ions. *Int. J. Mass Spectrom.* **1999**, *188* (1–2), 121–130.
(37) Lee, J. W.; Davidson, K. L.; Bush, M. F.; Kim, H. I. Collision Cross Sections and Ion Structures: Development of a General Calculation Method via High-Quality Ion Mobility Measurements and Theoretical Modeling. *Analyst* **2017**, *142* (22), 4289–4298.
(38) Von Helden, G.; Wyttenbach, T.; Bowers, M. T. Conformation of Macromolecules in the Gas Phase: Use of Matrix-Assisted Laser Desorption Methods in Ion Chromatography. *Science* **1995**, *267* (5203), 1483–1485.
(39) Ude, S.; Fernández De La Mora, J.; Thomson, B. A. Charge-Induced Unfolding of Multiply Charged Polyethylene Glycol Ions. *J. Am. Chem. Soc.* **2004**, *126* (38), 12184–12190.
(40) Trimpin, S.; Plasencia, M.; Isailovic, D.; Clemmer, D. E. Resolving Oligomers from Fully Grown Polymers with IMS–MS. *Anal. Chem.* **2007**, *79* (21), 7965–7974.
(41) Alessi, M. L.; Norman, A. I.; Knowlton, S. E.; Ho, D. L.; Greer, S. C. Helical and Coil Conformations of Poly(Ethylene Glycol) in Isobutyric Acid and Water. *Macromolecules* **2005**, *38* (22), 9333–9340.
(42) Tonelli, A. E. PLLA in Solution: A Flexible Random-Coil or an Extended, Rather Rigid Helical Polymer. *Macromolecules* **2014**, *47* (17), 6141–6143.
(43) Hudgins, R. R.; Jarrold, M. F. Helix Formation in Unsolvated Alanine-Based Peptides: Helical Monomers and Helical Dimers. *J. Am. Chem. Soc.* **1999**, *121* (14), 3494–3501.
(44) Wang, D.; Chen, K.; Kulp, J. L.; Arora, P. S. Evaluation of Biologically Relevant Short α-Helices Stabilized by a Main-Chain Hydrogen-Bond Surrogate. *J. Am. Chem. Soc.* **2006**, *128* (28), 9248–9256.
(45) Jas, G. S.; Kuczera, K. Equilibrium Structure and Folding of a Helix-Forming Peptide: Circular Dichroism Measurements and Replica-Exchange Molecular Dynamics Simulations. *Biophys. J.* **2004**, *87* (6), 3786–3798.
(46) Kohtani, M.; Jarrold, M. F.; Wee, S.; O'Hair, R. A. J. Metal Ion Interactions with Polyalanine Peptides. *J. Phys. Chem. B* **2004**, *108* (19), 6093–6097.

(47) Hudgins, R. R.; Mao, Y.; Ratner, M. A.; Jarrold, M. F. Conformations of GlynH+ and AlanH+ Peptides in the Gas Phase. *Biophys. J.* **1999**, *76* (3), 1591−1597.
(48) Itagaki, H.; Yoshida, N.; Sano, T.; Yokoyama, M.; Iba, N.; Sugiyama, R.; Kuroki, M. Electrically Conductive Gels Prepared from Syndiotactic Polystyrene and an Ionic Liquid. *ACS Omega* **2019**, *4* (14), 16125−16129.
(49) Zatorska-Płachta, M.; Łazarski, G.; Maziarz, U.; Foryś, A.; Trzebicka, B.; Wnuk, D.; Chołuj, K.; Karewicz, A.; Michalik, M.; Jamróz, D.; Kepczynski, M. Encapsulation of Curcumin in Polystyrene-Based Nanoparticles—Drug Loading Capacity and Cytotoxicity. *ACS Omega* **2021**, *6* (18), 12168−12178.
(50) Burguière, C.; Dourges, M.-A.; Charleux, B.; Vairon, J.-P. Synthesis and Characterization of ω-Unsaturated Poly(Styrene- *b* - *n* -Butyl Methacrylate) Block Copolymers Using TEMPO-Mediated Controlled Radical Polymerization. *Macromolecules* **1999**, *32* (12), 3883−3890.
(51) Ladavière, C.; Lacroix-Desmazes, P.; Delolme, F. First Systematic MALDI/ESI Mass Spectrometry Comparison to Characterize Polystyrene Synthesized by Different Controlled Radical Polymerizations. *Macromolecules* **2009**, *42* (1), 70−84.
(52) Gruendling, T.; Hart-Smith, G.; Davis, T. P.; Stenzel, M. H.; Barner-Kowollik, C. Enhanced Ionization in Electrospray Ionization Mass Spectrometry of Labile End-Group-Containing Polystyrenes Using Silver(I) Tetrafluoroborate as Doping Salt. *Macromolecules* **2008**, *41* (6), 1966−1971.
(53) Altintas, O.; Josse, T.; De Winter, J.; Matsumoto, N. M.; Gerbaux, P.; Wilhelm, M.; Barner-Kowollik, C. Ready Access to End-Functional Polystyrenes via a Combination of ARGET ATRP and Thiol−Ene Chemistry. *Polym. Chem.* **2015**, *6* (39), 6931−6935.
(54) Gidden, J.; Bowers, M. T.; Jackson, A. T.; Scrivens, J. H. Gas-Phase Conformations of Cationized Poly(Styrene) Oligomers. *J. Am. Soc. Mass Spectrom.* **2002**, *13* (5), 499−505.
(55) Izuagbe, A. E.; Truong, V. X.; Tuten, B. T.; Roesky, P. W.; Barner-Kowollik, C. Visible Light Switchable Single-Chain Nanoparticles. *Macromolecules* **2022**, *55* (20), 9242−9248.
(56) Gerber, J.; Radke, W. Topological Separation of Linear and Star-Shaped Polystyrenes by off-Line 2D Chromatography. Stars Having High Molar Mass Arms and Quantification of the Star Fraction. *Polymer* **2005**, *46* (22), 9224−9229.
(57) Duez, Q.; Chirot, F.; Liénard, R.; Josse, T.; Choi, C.; Coulembier, O.; Dugourd, P.; Cornil, J.; Gerbaux, P.; De Winter, J. Polymers for Traveling Wave Ion Mobility Spectrometry Calibration. *J. Am. Soc. Mass Spectrom.* **2017**, *28* (11), 2483−2491.
(58) Gabelica, V.; Shvartsburg, A. A.; Afonso, C.; Barran, P.; Benesch, J. L. P.; Bleiholder, C.; Bowers, M. T.; Bilbao, A.; Bush, M. F.; Campbell, J. L.; Campuzano, I. D. G.; Causon, T.; Clowers, B. H.; Creaser, C. S.; De Pauw, E.; Far, J.; Fernandez-Lima, F.; Fjeldsted, J. C.; Giles, K.; Groessl, M.; Hogan, C. J.; Hann, S.; Kim, H. I.; Kurulugama, R. T.; May, J. C.; McLean, J. A.; Pagel, K.; Richardson, K.; Ridgeway, M. E.; Rosu, F.; Sobott, F.; Thalassinos, K.; Valentine, S. J.; Wyttenbach, T. Recommendations for Reporting Ion Mobility Mass Spectrometry Measurements. *Mass Spectrom. Rev.* **2019**, *38* (3), 291−320.
(59) *Materials Studio*; BIOVIA - Dassault Systèmes: San Diego, 2022.
(60) Pugh, T. L.; Heller, W. Density of Polystyrene and Polyvinyltoluene Latex Particles. *Journal of Colloid Science* **1957**, *12* (2), 173−180.
(61) Mesleh, M. F.; Hunter, J. M.; Shvartsburg, A. A.; Schatz, G. C.; Jarrold, M. F. Structural Information from Ion Mobility Measurements: Effects of the Long-Range Potential. *J. Phys. Chem.* **1996**, *100* (40), 16082−16086.
(62) Ewing, S. A.; Donor, M. T.; Wilson, J. W.; Prell, J. S. Collidoscope: An Improved Tool for Computing Collisional Cross-Sections with the Trajectory Method. *J. Am. Soc. Mass Spectrom.* **2017**, *28* (4), 587−596.
(63) Frisch, M. J.; Trucks, G. W.; Schlegel, H. B.; Scuseria, G. E.; Robb, M. A.; Cheeseman, J. R., Scalmani, G.; Barone, V.; Mennucci, B.; Petersson, G. A. *Gaussian2009*; Gaussian, Inc., 2009.
(64) Duez, Q.; Van Huizen, N. A.; Lemaur, V.; De Winter, J.; Cornil, J.; Burgers, P. C.; Gerbaux, P. Silver Ion Induced Folding of Alkylamines Observed by Ion Mobility Experiments. *Int. J. Mass Spectrom.* **2019**, *435*, 34−41.
(65) Grimme, S.; Antony, J.; Ehrlich, S.; Krieg, H. A Consistent and Accurate *Ab Initio* Parametrization of Density Functional Dispersion Correction (DFT-D) for the 94 Elements H-Pu. *J. Chem. Phys.* **2010**, *132* (15), 154104.
(66) Shoeib, T.; Cunje, A.; Hopkinson, A. C.; Siu, K. W. M. Gas-Phase Fragmentation of the Ag^+ —Phenylalanine Complex: Cation—π Interactions and Radical Cation Formation. *J. Am. Soc. Mass Spectrom.* **2002**, *13* (4), 408−416.
(67) Duez, Q.; Josse, T.; Lemaur, V.; Chirot, F.; Choi, C. M.; Dubois, P.; Dugourd, P.; Cornil, J.; Gerbaux, P.; De Winter, J. Correlation between the Shape of the Ion Mobility Signals and the Stepwise Folding Process of Polylactide Ions: Stepwise Folding Process of Polylactide Ions. *J. Mass Spectrom.* **2017**, *52* (3), 133−138.
(68) Saintmont, F.; De Winter, J.; Chirot, F.; Halin, E.; Dugourd, P.; Brocorens, P.; Gerbaux, P. How Spherical Are Gaseous Low Charged Dendrimer Ions: A Molecular Dynamics/Ion Mobility Study? *J. Am. Soc. Mass Spectrom.* **2020**, *31* (8), 1673−1683.
(69) Weber, P.; Hoyas, S.; Halin, É.; Coulembier, O.; De Winter, J.; Cornil, J.; Gerbaux, P. On the Conformation of Anionic Peptoids in the Gas Phase. *Biomacromolecules* **2022**, *23* (3), 1138−1147.
(70) Hoyas, S.; Halin, E.; Lemaur, V.; De Winter, J.; Gerbaux, P.; Cornil, J. Helicity of Peptoid Ions in the Gas Phase. *Biomacromolecules* **2020**, *21* (2), 903−909.
(71) Hoyas, S.; Weber, P.; Halin, E.; Coulembier, O.; De Winter, J.; Cornil, J.; Gerbaux, P. Helical Peptoid Ions in the Gas Phase: Thwarting the Charge Solvation Effect by H-Bond Compensation. *Biomacromolecules* **2021**, *22* (8), 3543−3551.
(72) Giles, K.; Williams, J. P.; Campuzano, I. Enhancements in Travelling Wave Ion Mobility Resolution. *Rapid Commun. Mass Spectrom.* **2011**, *25* (11), 1559−1566.
(73) Ruotolo, B. T.; Benesch, J. L. P.; Sandercock, A. M.; Hyung, S.-J.; Robinson, C. V. Ion Mobility−Mass Spectrometry Analysis of Large Protein Complexes. *Nat. Protoc* **2008**, *3* (7), 1139−1152.
(74) Duez, Q.; Hoyas, S.; Josse, T.; Cornil, J.; Gerbaux, P.; De Winter, J. Gas-phase Structure of Polymer Ions: Tying Together Theoretical Approaches and Ion Mobility Spectrometry. *Mass Spectrom. Rev.* **2023**, *42* (4), 1129−1151.
(75) Lee, B.; Richards, F. M. The Interpretation of Protein Structures: Estimation of Static Accessibility. *J. Mol. Biol.* **1971**, *55* (3), No. 379.
(76) Mahadevi, A. S.; Sastry, G. N. Cation−π Interaction: Its Role and Relevance in Chemistry, Biology, and Material Science. *Chem. Rev.* **2013**, *113* (3), 2100−2138.